International Journal of Pharmaceutics: X 5 (2023) 100152

Contents lists available at ScienceDirect

International Journal of Pharmaceutics: X

journal homepage: www.sciencedirect.com/journal/international-journal-of-pharmaceutics-x

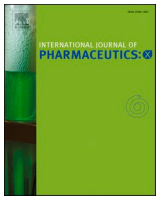

Investigation on the use of fused deposition modeling for the production of IR dosage forms containing Timapiprant

Marco Uboldi [a], Arianna Chiappa [b,c], Marisa Pertile [d], Alessandro Piazza [d], Stefano Tagliabue [c], Anastasia Foppoli [a], Luca Palugan [a,*], Andrea Gazzaniga [a], Lucia Zema [a], Alice Melocchi [a]

[a] Sezione di Tecnologia e Legislazione Farmaceutiche "Maria Edvige Sangalli", Dipartimento di Scienze Farmaceutiche, Università degli Studi di Milano, via Giuseppe Colombo 71, 20133 Milano, Italy
[b] Consorzio Interuniversitario Nazionale per la Scienza e Tecnologia dei Materiali (INSTM), via Giuseppe Giusti 9, 50121 Firenze, Italy
[c] Dipartimento di Chimica, Materiali e Ingegneria Chimica "G. Natta", Politecnico di Milano, Piazza Leonardo da Vinci 32, 20133 Milano, Italy
[d] Chiesi Farmaceutici S.p.A., Largo Francesco Belloli 11/A, 43122 Parma, Italy

ARTICLE INFO

Keywords:
3D printing
Immediate release
Oral administration
BCS class II drug
Personalized therapy
Dissolution
Pycnometric analysis

ABSTRACT

The present work focused on evaluating the feasibility of fused deposition modeling (FDM) in the development of a dosage form containing Timapiprant (TMP), also known as CHF6532, which is a novel active molecule indicated in the potential treatment of eosinophilic asthma upon oral administration. The resulting product could be an alternative, with potential towards personalization, of immediate release (IR) tablets used in the clinical studies. Formulations based on different polymeric carriers were screened, leading to the identification of a polyvinyl alcohol-based one, which turned out acceptable for versatility in terms of active ingredient content, printability and dissolution performance (*i.e.* capability to meet the dissolution specification set, envisaging >80% of the drug dissolved within 30 min). Following an in-depth evaluation on the influence of TMP solid state and of the voids volume resulting from printing on dissolution, few prototypes with shapes especially devised for therapy customization were successfully printed and were compliant with the dissolution specification set.

1. Introduction

Over the past 10 years, the number of research studies focused on the application of three dimensional (3D) printing by fused deposition modeling (FDM) in pharmaceutics has definitely grown, likely due to the cost-accessibility of desktop equipment and of the overall simplicity of the technique, even for unexperienced users [Aho et al., 2019; Dumpa et al., 2021; Fuenmayor et al., 2018; Gupta et al., 2022; Joo et al., 2020; Melocchi et al., 2020a]. Indeed, FDM is an extrusion-based additive process in which filaments, composed of thermoplastic polymeric formulations and obtained by hot melt extrusion (HME), are deposited through a nozzle in a series of overlapping layers on a build plate, following a software-controlled path [Krueger et al., 2022; Parulski et al., 2021; Quodbach et al., 2022]. In this respect, the mutual movement of the printhead and of the build plate in x-, y- and z-directions enables the fabrication of the product bottom up, layer-by-layer.

The evolution of this technique prompted by its application to the development of drug products has entailed not only a rapid increase in the type/number of starting materials employed, but also a marked improvement in the strategies to predict and control the printing process as well as in the methods for the characterization, even in real-time, of the printed products. Moreover, as progresses attained through a trial-and-error procedure would be highly expensive and time-consuming, the possibility to couple 3D printing with quality by design approaches, machine learning and mathematical models able to identify connections between inputs and features of the resulting products was preliminarily investigated [Dos Santos et al., 2021; Edinger et al., 2018; Elbadawi et al., 2020, 2021a, 2021b; Henry et al., 2021; Linares et al., 2021; Melocchi et al., 2021a; Muñiz et al., 2021; Pires et al., 2020]. This was a necessary path to ensure, in the near future, the actual application of FDM to the manufacturing of safe, high-quality personalized drug products to be administered to patients.

In such a scenario, printed dosage forms intended for the oral route were probably the most studied, with scientists originally targeting the development of inert or hydrophilic prolonged release matrices [Caillleaux et al., 2021; Goyanes et al., 2015a; Shaqour et al., 2020; Tan et al., 2018]. Simple geometries were first considered but, acquiring deeper competences and confidence with the FDM technique, increasingly

* Corresponding author.
E-mail address: luca.palugan@unimi.it (L. Palugan).

https://doi.org/10.1016/j.ijpx.2022.100152
Received 28 September 2022; Received in revised form 19 December 2022; Accepted 22 December 2022
Available online 24 December 2022

Table 1
HME and FDM parameters relevant to drug-containing products (5–40% TMP) based on different polymeric formulations.

Polymeric formulation				HME			FDM
Polymer	Plasticizer	Soluble filler		T, °C	Screw speed, rpm	Torque, N·cm	T, °C
HPC	5% PEG 400			145	50	35	180
PEO				100	60	40	n.d.
KIR	15% GLY			160	80	70–130	185
HPMCAS	35% PEG 8000			160	30	20	190
SLP	15% PEG 400			110	40	60	150
KVA	0–25% PEG 400			95–150	30–40	50–300	n.d.
PVA	15% GLY			170	60	50–120	180
	15% GLY	30% EMD		145–120	50	55–80	160
	15% GLY	30% GIQ	15% GLY	150	40	100	170
	15% GLY	30% TCK	15% GLY	180	40	70	200

n.d.: not defined because the filaments obtained were unsuitable for printing.

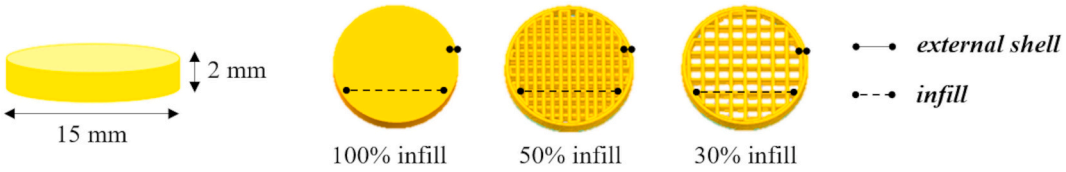

Fig. 1. Virtual models of the screening specimens with dimensional details and different infill percentages.

Table 2
FDM conditions kept constant for all the printing trials.

Extrusion multiplier	1.00
Layer height, mm	0.225
Perimeter shells for each layer	1
Printing speed, mm/s	25
First layer underspeed, %	10
Additions	skirt
Skirt Layers	1
Skirt Outlines	2
Build plate temperature, °C	50

complex designs and release kinetics were attained, ranging from hollow and multi-compartment systems to devices showing self-transformation of their shape over time, thus resulting in 4D printing [Dumpa et al., 2021; Goyanes et al., 2015b, 2015c; Maroni et al., 2020; Melocchi et al., 2020b, 2021b; Uboldi et al., 2021, 2022; Palugan et al., 2021; Parulski et al., 2021]. However, one of the main focus of the research is still represented by the development of immediate release (IR) dosage forms, which would in principle result in a personalized alternative to mass-produced tablets. [Crișan et al., 2022; Duranović et al., 2021; Fanous et al., 2021; Li et al., 2020; Than and Titapiwatanakun, 2021]. As they currently possess the greatest number of shares in the pharmaceutical market, while printed products could easily be conceived around the needs of specific patients - for instance in terms of design, drug strength, excipient composition and even flavor - FDM of IR dosage forms could represent an attractive development strategy to be pursued from the industry point of view [Cailleaux et al., 2021; Seoane-Viaño et al., 2021; Okwuosa et al., 2021; Trenfield et al., 2018, 2020; Vaz and Kumar, 2021; Wang et al., 2021]. In this regard, increasing the involvement of pharmaceutical companies in the development of 3D printed products could be aimed at enhancing therapy adherence and reducing relevant side effects, as well as implementing new processes in their portfolio, while working with active ingredients that may be strategic [Fanous et al., 2020; Markl et al., 2018; Smith et al., 2018a, 2018b].

Timapiprant (TMP), also identified as CHF6532, is a drug molecule originally developed by a clinical stage biotechnology company (Atopix therapeutics limited), which was acquired by Chiesi Farmaceutici S.p.A in 2016. It was expected to address unmet needs in respiratory medicine, particularly in eosinophilic airway diseases associated with type 2 inflammation and thus with a marked increase in type 2 cytokines

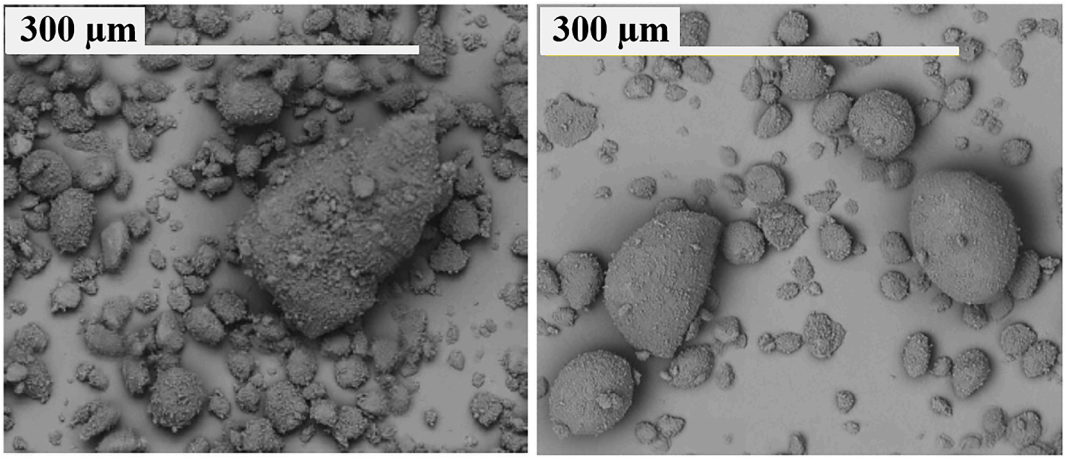

Fig. 2. SEM images of TMP powder.

Table 3
Mass, TMP content and dissolution characteristics of printed screening specimens with relevant coefficient of variation (CV).

Polymeric formulation	Infill, %	TMP, %	Mass, mg (CV)	$t_{80\%}$, min (CV)
HPC + 5% PEG 400	100	5	394.79 (3.65)	89.65 (7.05)
		40		
	30	5	184.47 (1.19)	22.24 (3.49)
		40		
KIR + 15% GLY	100	5	336.58 (4.81)	21.56 (13.54)
		40	437.29 (3.98)	42.80 (5.78)
	30	5	158.44 (7.00)	14.07 (6.75)
		40	225.43 (1.81)	43.76 (14.18)
HPMCAS + 35% PEG 8000	100	5	425.77 (8.73)	>120
		40		
	30	5	183.96 (5.21)	>120
		40		
SLP + 15% PEG 400	100	5	418.28 (1.50)	>120
		40	384.67 (5.34)	>120
	30	5	137.41 (3.49)	>120
		40	172.62 (6.08)	>120
PVA + 15% GLY	100	5	486.02 (3.79)	>120
		40	372.27 (2.40)	57.69 (5.32)
	30	5	184.15 (2.76)	19.02 (20.91)
		40	164.38 (3.38)	13.23 (14.00)
30% EMD	100	5	380.16 (8.50)	80.41 (15.14)
		40	378.19 (6.68)	72.50 (20.84)
	30	5	164.62 (5.23)	11.78 (8.82)
		40	226.56 (1.99)	17.16 (21.16)
30% GIQ + 15% GLY	100	5	391.47 (6.31)	63.83 (23.92)
		40	490.21 (3.10)	64.94 (7.45)
	30	5	154.56 (5.81)	10.89 (13.27)
		40	490.21 (3.10)	14.47 (9.80)
30% TCK + 15% GLY	100	5	414.61 (3.97)	105.29 (17.57)
		40	452.32 (3.98)	107.53 (23.06)
	30	5	174.49 (7.24)	14.08 (22.81)
		40	221.77 (4.83)	16.19 (5.10)

interleukins (*e.g.* IL-4, IL-5, IL-13) [https://www.chiesi.com/img/annual_report/documenti/ mZQpMHoqnWAnR_2016_ENG_SD.pdf; Lommatzsch, 2020; Shrimanker et al., 2019; Singh et al., 2013]. Therefore, TMP could be employed in hard-to-treat pathologies being formulated in oral, patient-friendly products. In this respect, tablets were developed and used in clinical phase III studies [https://clinicaltrials.gov/ct2/show/NCT04049175]. However, TMP is a high-melting practically insoluble BCS class II compound, whose formulation in IR dosage forms by hot-processing should be particularly critical. Various attempts have been described in the literature to ensure the attainment of IR performance from FDM printed dosage forms, including composition, design and manufacturing approaches [Arafat et al., 2018; Duranović et al., 2021; Goyanes et al., 2015a, 2015c; Gültekin et al., 2019; Ilyés et al., 2019; Isreb et al., 2019; Solanki et al., 2018; Sadia et al., 2016, 2018; Shi et al., 2021]. A range of excipients were included into the filament composition, such as soluble fillers and disintegrants. This formulation approach was coupled with the identification of unique product shapes/geometries, which are definitely not feasible *via* more traditional manufacturing processes. Thus, solid units characterized by voids and channels as well as by extended surface available for interaction with biological fluids were described (*e.g.* radiator-like systems). Finally, different FDM parameters were demonstrated essential in modulating the behavior of the final products upon contact with aqueous media, such as infill percentage and relevant shape, number of external shells and presence of top and bottom layers [Curti et al., 2020; Goyanes et al., 2015a; Melocchi et al., 2021c; Tagami et al., 2017; Yang et al., 2018].

Table 4
$t_{80\%}$ data relevant to printed, extruded and milled samples (< 355 μm size fraction) based on PVA and containing increasing amount of TMP.

TMP (%)	$t_{80\%}$, min (CV)		
	Printed units 30% infill	Extruded samples	Milled extruded samples
5	19.02 (20.92)	78.93 (9.54)	11.49 (11.24)
25	17.15 (6.62)	71.81 (4.37)	5.43 (12.22)
40	13.23 (14.00)	51.49 (10.43)	7.62 (12.49)

Based on these premises, the aim of the present work was to evaluate the feasibility of FDM in the manufacturing of TMP-containing IR solid dosage forms with a potential towards personalization, for instance in terms of shape, composition and active ingredient load. In this respect, a simple formulation was identified and its versatility in terms of composition and printability was evaluated. A thorough investigation of the influence of FDM conditions on the dissolution performance of printed samples was also undertaken.

2. Materials and methods

2.1. Materials

TMP (water solubility ≈ 50 ng/mL; agglomerated particles (sieved fraction <355 μm) consisting of sub-micrometric size crystals with Dv90 < 1 μm); Chiesi Farmaceutici S.p.A., Parma, I); low viscosity hydroxypropyl cellulose (NISSO HPC SSL, Nisso Chemical Europe GmbH, Duesseldorf, D; HPC); hydroxypropyl methyl cellulose acetate succinate (AQUOT-LG®; Shin-Etsu, Tokyo, J; HPMCAS); polyethylene oxide (Sentry Polyox™ WSR N10 LEO NF, Dupont, Paris, F; PEO); low viscosity polyvinyl alcohol (Gohsenol® EG 03P, Mitsubishi Chemicals, Tokyo, J; PVA); polyvinyl alcohol-polyethylene glycol graft copolymer (Kollicoat® IR, BASF, Ludwigshafen, D; KIR); polyvinyl caprolactam-polyvinyl acetate-polyethylene glycol graft *co*-polymer (Soluplus®, BASF, Ludwigshafen, D; SLP); polyvinylpyrrolidone (Kollidon® VA 64, BASF, Ludwigshafen, D; KVA); glycerol (Pharmagel, Milan, I; GLY); polyethylene glycols with different molecular weights (Clariant Masterbatches, Milan, I;, PEG 400 and PEG 8000, respectively); Dextrates (EMDEX®, JRS Pharma, Rosenberg, D; EMD); Isomalt (GalenIQ™ 810, Beneo-Palatinit GmbH, Mannheim, D; GIQ); Potato dextrins (Tackidex®, Roquette, Lestrem, F; TCK); Cetrimonium bromide (VWR International, Milan, I; CTAB).

2.2. Methods

2.2.1. Powder mixture preparation

All materials, except for PEGs and GLY, were kept in an oven at 40 °C for 24 h before use.

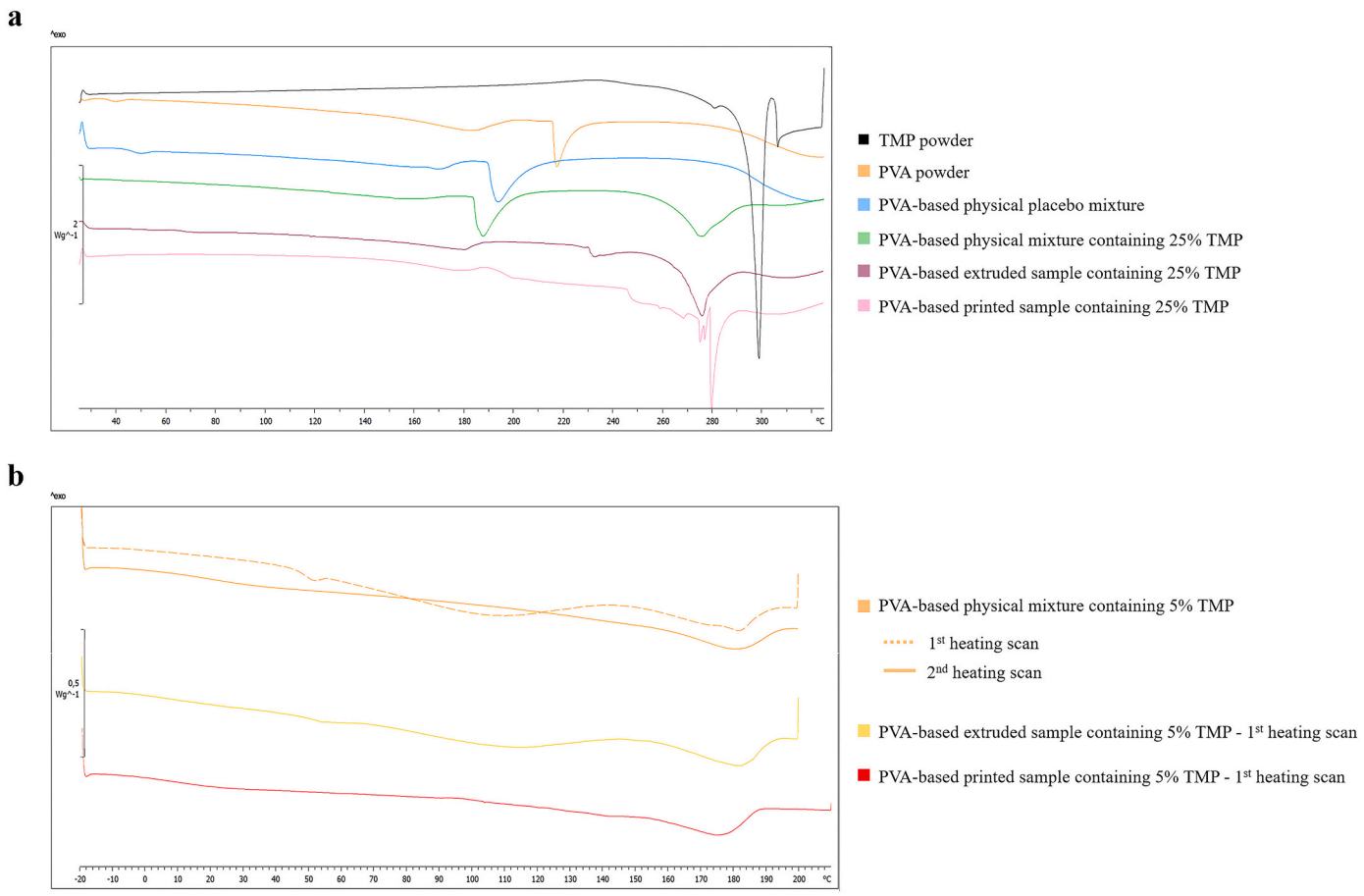

Fig. 3. DSC data relevant to different samples which were subjected to a) a single heating scan up to 325 °C and b) a protocol comprising a sequence of heating/cooling/heating, up to 210 °C.

Plasticized polymeric formulations (Table 1) were prepared by mixing in a mortar the polymer with the selected plasticizer. The amount of the latter was expressed as % *w*/w on the dry polymer. PVA-based formulations containing soluble fillers (30% w/w on the final formulation) were also prepared. As far as EMD and GIQ fillers are concerned, they were first added into the liquid plasticizer before mixing with the polymer.

Drug-containing formulations were obtained by mixing in a mortar the desired quantity of TMP with the selected plasticized polymeric formulation previously prepared. TMP is produced by spherical agglomeration technology with a large particle size distribution (up to 500–600 μm), therefore the >355 μm fraction was discarded to avoid clogging of the printer nozzle. The amount of the drug was calculated as % w/w on the plasticized polymeric formulation, so as mixture containing increasing amounts of TMP were prepared (5–40% w/w range).

2.2.2. Hot melt extrusion

Starting from the drug-containing formulations, filaments intended for feeding the FDM printer were prepared by HME using a twin-screw extruder (Haake™ MiniLab II, Thermo Scientific, Madison, US-WI), as before described [Melocchi et al., 2019a, 2019b]. The extruder was equipped with counter-rotating screws and a rod-shaped die, which was custom-made in aluminum (ø = 1.80 mm). Process conditions were set for each polymeric formulation and it was not necessary to change them by modifying the TMP load or the amount of soluble filler (Table 1). Extruded filaments were manually pulled and forced to pass through a caliper connected to the extruder and set at 1.75 mm [Melocchi et al., 2016]. After production, filament diameter was verified every 5 cm in length and portions out from the acceptable range (1.75 ± 0.05 mm) were discarded. Filaments were kept in oven at 40 °C until use, except for PEO-, KIR- and SLP-based ones which were stored in a desiccator with silica. Relevant portions having different lengths (50–70 mm) were also cut to achieve samples with a weight comparable to that of printed screening prototypes having the same composition. These were stored separately and identified as extruded samples. Samples of the filaments were also subjected to a milling step (pin mill Retsch ZM200, Dusseldorf, D; 800 mg of starting material, speed set at 6000 rpm for 5 s). To avoid melting of the material during this step a first run was performed with a 1 mm mesh, followed by a second one carried out using a 500 μm mesh. The milled product was sieved and powder samples <355 μm with a weight comparable to that of printed screening prototypes having the same composition were collected and identified as milled extruded samples.

2.2.3. 3D printing

FDM products (*i.e.* screening specimens and final prototypes) were printed by a Kloner3D 240® Twin (Kloner3D, Florence, I) equipped with 0.5 mm nozzle. Computer-aided design (CAD) files were purposely prepared using Autodesk® Autocad® 2016 software version 14.0 (Autodesk Inc., San Francisco, US-CA). Electronic models were saved in .stl format and imported into the printer software (Simplify 3D, Milan, I). CAD files of screening units were designed in the form of simple cylinders (Fig. 1). Electronic models of the final prototypes are reported in the Results and Discussion Section. The printing temperature was fine-tuned based on the behavior of the various filaments during initial printing trials in order to ensure continuous deposition of the material and to avoid detachment of successive layers when printing the object, thus resulting in a non-coherent structure. Apart from the temperature,

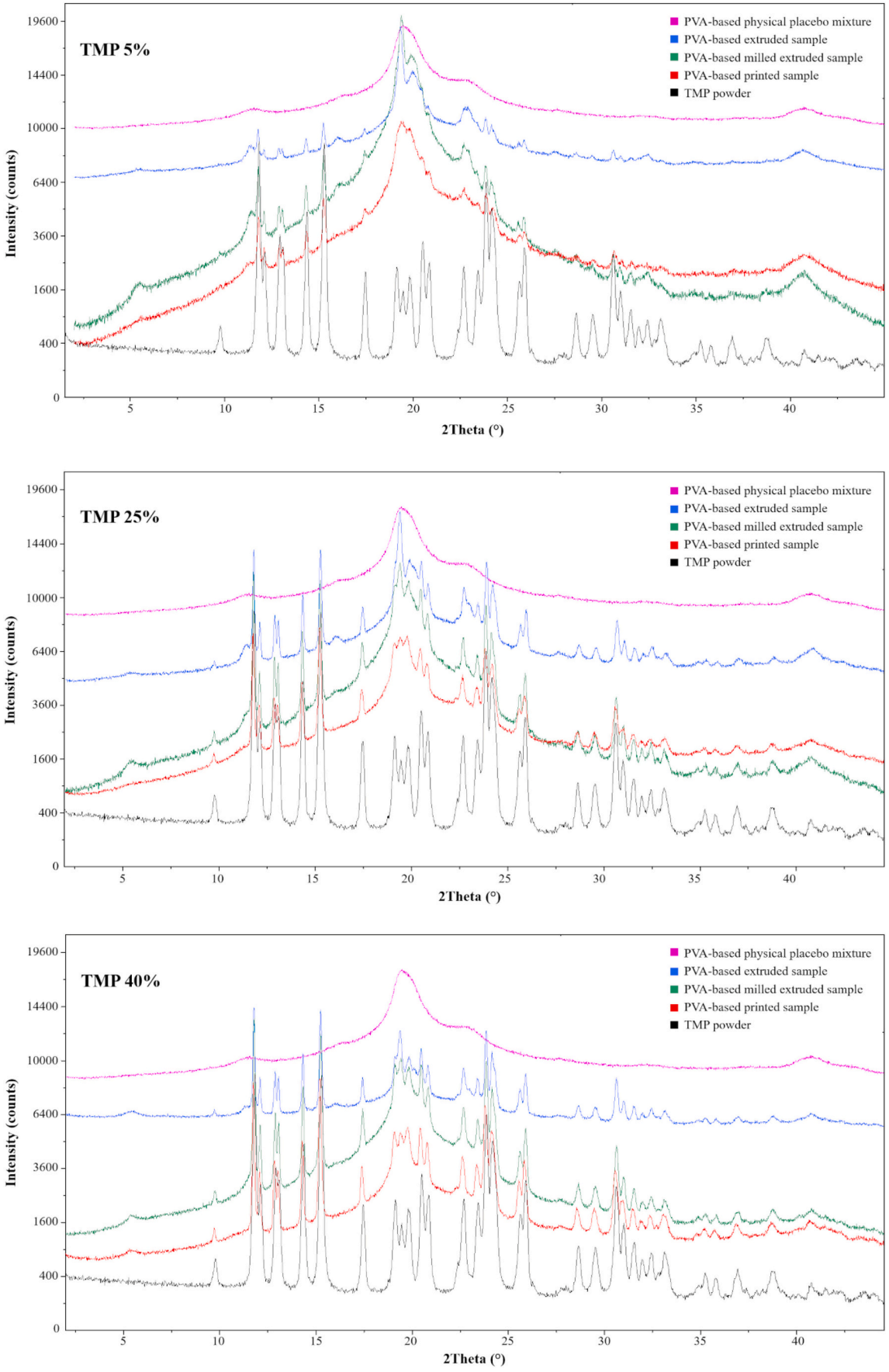

Fig. 4. XRD spectra relevant to various PVA-based samples.

Table 5
Mass, pycnometric density and porosity data relevant to PVA-based printed screening specimens.

TMP (%)	Mass, mg (CV)			Pycnometric density, mg/mm^3 (CV)			Porosity, % (CV)		
	Infill, %			Infill, %			Infill, %		
	100	50	30	100	50	30	100	50	30
5	486.02 (3.79)	280.88 (5.84)	184.15 (2.76)	1.30 (0.17)	1.35 (0.91)	1.40 (0.76)	14.88 (14.70)	46.52 (7.85)	62.80 (3.69)
25	452.78 (1.74)	253.22 (3.71)	193.62 (5.07)	1.30 (0.36)	1.36 (0.33)	1.41 (0.58)	9.63 (14.68)	50.78 (5.28)	65.07 (4.59)
40	372.27 (2.40)	200.24 (5.70)	164.38 (3.38)	1.33 (0.17)	1.36 (0.91)	1.36 (0.76)	24.84 (7.58)	59.62 (4.86)	61.06 (4.80)

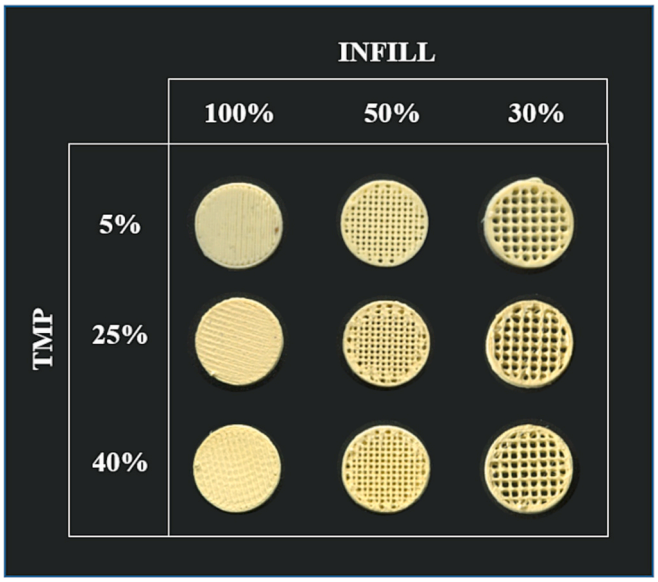

Fig. 5. photographs of printed screening specimens having diverse infill and TMP content.

which was set according to the polymeric vehicle (Table 1), main printing conditions were kept constant for all the formulations investigated to attain products with satisfactory characteristics (Table 2). These were fabricated by setting diverse infill percentages, while always printing the object with a single external shell for each layer (Fig. 1). The printing profile was implemented with a skirt consisting of two outlines, which was added to the first layer in order to improve the adhesion of the unit under fabrication to the build plate. Adhesion was promoted by keeping the temperature of the build plate at 50 °C, using a paper tape and reducing the printing speed. Before processing a new formulation, the nozzle was disassembled and cleaned, so that the z value needed to be reset.

2.2.4. Characterization of products

2.2.4.1. Mass and dimensions. Printed products were checked for mass (analytical balance BP211, Sartorius, Ulm, D; $n = 6$) and dimensions (*i.e.* height and diameter; Digital caliper, Mitutoyo, Kawasaki, J). Data relevant to cylindrical screening specimens were used to calculate the geometric volume (*i.e.* radius^2 * 3,14 * height). Images of the samples were acquired (Epson scan 4800, Milan, I; 24 bit images, resolution 4800 dpi).

2.2.4.2. Thermal analysis. Thermal analysis was carried out using differential scanning calorimetry (DSC Discovery, TA Instruments, New Castle, US-DE; DSC Stare System 1, Mettler-Toledo, Milan, I). Samples were accurately weighed (3–5 mg) and analyzed in closed aluminum pans. The tests were performed under nitrogen atmosphere setting two different protocols:

(i) a single heating ramp (from 25 °C to 325 °C, rate 10 °C /min);
(ii) sample was first heated from 25 °C to 210 °C, then cooled to −20 °C and reheated to 210 °C (rate 7 °C /min)

2.2.4.3. X-ray diffraction. X-ray diffraction experiments were performed using X-ray diffractometer (Empyrean V2.0, Malvern panalytical, Monza, I) equipped with Cu radiation source (Cu Kα 1.5406 Å). Samples were analyzed between Kapton foils and spun with revolution time of 1 s. The measurements were performed in transmission mode, 2Theta scan from 2 to 45°, step size 0.01°, time per step 239 s, soller slit 0.02 rad, divergence slit 1/2°, antiscatter slit 1/2°.

2.2.4.4. Volume. Pycnometric volume was evaluated by gas pycnometer (Pycnomatic ATC, Thermo Fisher Scientific, Monza, I), performing the analyses according to the ASTM D6226 standard and taking three consecutive measurements on each sample. Considering samples of a known mass, this volume excludes the volume occupied by open pores, while it includes that occupied by sealed pores or pores inaccessible to the gas (European Pharmacopoeia 10.5 Ed., Monograph 2.9.23 Gas pycnometric density of solids). Experiments were carried out in pure helium atmosphere (Helium 5.0, purity grade), at 23 °C and at an

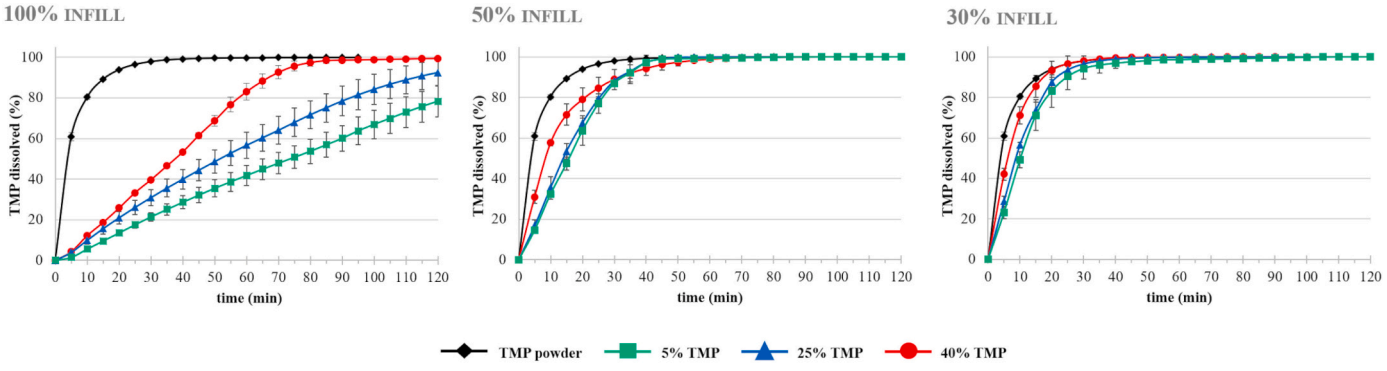

Fig. 6. dissolution profiles relevant to TMP powder as such and PVA-based printed samples having diverse infill and drug content.

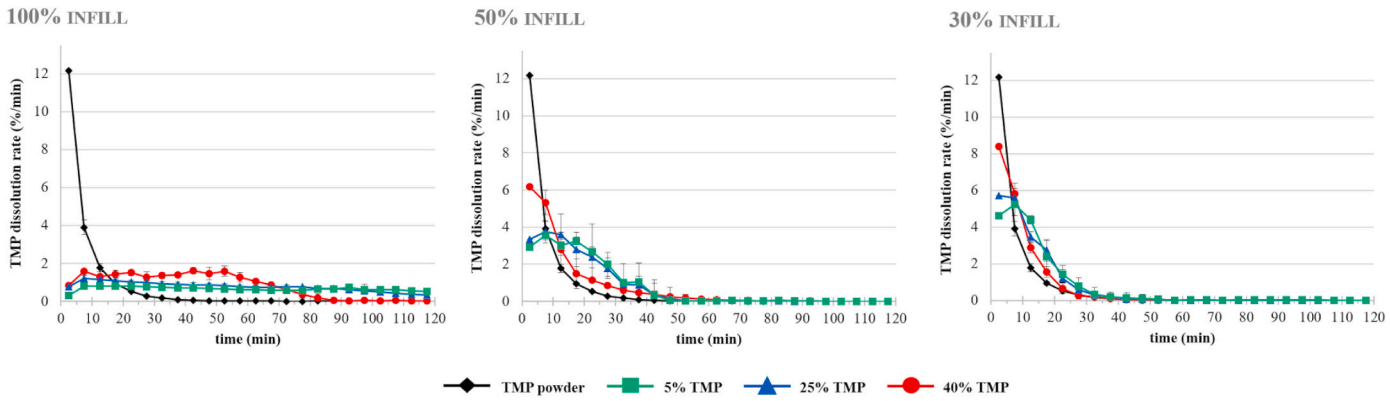

Fig. 7. dissolution rate profiles relevant to TMP powder as such and PVA-based printed samples having diverse infill and drug content.

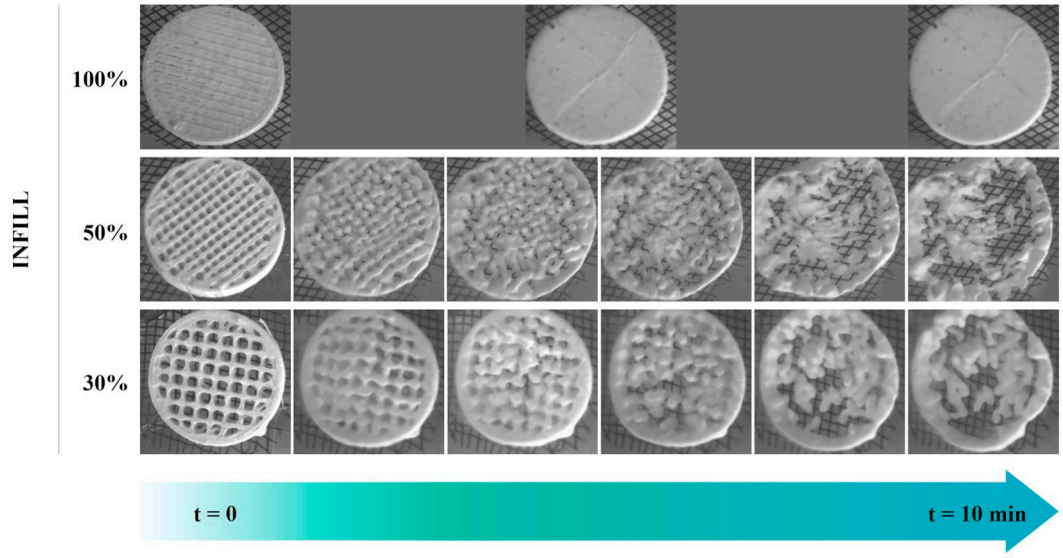

Fig. 8. photographs of PVA-based samples, having 40% nominal TMP content and printed with diverse infill, during interaction with the dissolution medium

equilibrium pressure of 2 kPa. From the data collected, the following parameters were calculated:

$$pycnometric\ density = \frac{mass}{pycnometric\ volume} \quad (1)$$

$$porosity = \frac{geometric\ volume - pycnometric\ volume}{geometric\ volume} \times 100 \quad (2)$$

2.2.4.5. Dissolution performance and drug content. Dissolution test was carried out by a USP apparatus II (Distek, North Brunswick Township, US-NJ), according to a procedure ensuring sink conditions. The test, lasting for 120 min, entailed 900 mL of sodium phosphate buffer (pH 6.8) containing 0.4% *w/V* of CTAB, kept at 37 ± 0.5 °C. The dissolution apparatus (paddle, 75 rpm) was connected to a pump (IPC Ismatec™, Thermo Fisher Scientific, Monza, I) for the automatic collection of fluid samples and to a spectrophotometer for relevant assay (Lambda 35, Perkin Elmer, Milan, I; 1 mm cuvette path length, 231 nm λ_{max}). The amount of TPM dissolved at each time point was determined from a calibration curve purposely built ($y = 16.484\times + 0.0064$, $R^2 = 0.9998$).

TMP actual content was assessed spectrophotometrically after dissolving the samples in 900 mL of the same medium used for the dissolution tests, while TMP nominal content was calculated as follows, taking into account the experimental weight of the tested sample:

$$a = \frac{b}{(1+c)} * c.$$

where

a = nominal load of TMP, mg
b = weight of the sample, mg
c = percentage of TMP

Dissolution data were expressed as percentage of TMP dissolved with respect to the amount of drug recovered in the dissolution medium at the end of the test (*i.e.* after 15 min ultra-turrax of the vessel content; VWR, Milan, I). Time to 80% dissolution ($t_{80\%}$) was calculated by linear interpolation of the dissolution data immediately before and after the time point of interest. Moreover, the rate of dissolution (r_{diss}) was calculated as the average value between two successive dissolution data points (*i.e.* every 5 min). The resulting value was plotted at the center of

Table 6
Design and dimensional details of the shapes under investigation.

	50% infill	30% infill
Cylinder	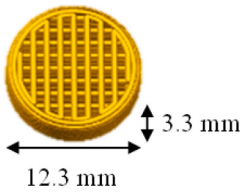	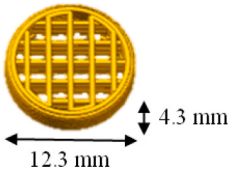
Drop	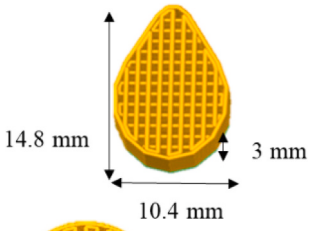	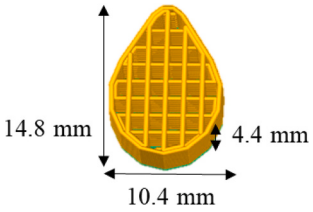
Swivel	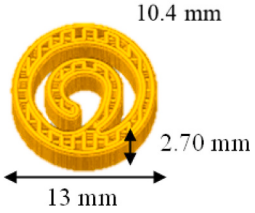	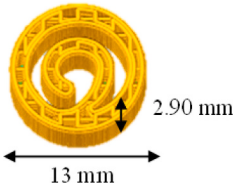
Spiral drop	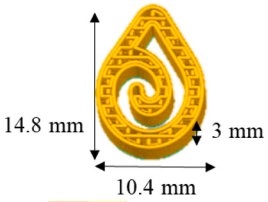	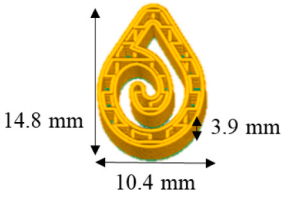
Hexagon	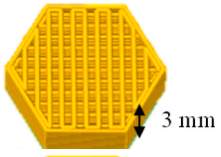	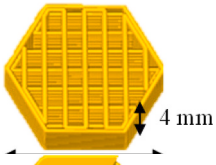
Company logo	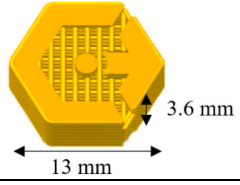	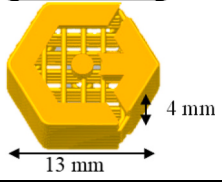

the relevant time interval.

High-resolution images of printed samples immersed in the dissolution medium, kept at 37 °C ± 0.5 °C and under stirring at 75 rpm, were taken at different time points (camera UI1490LE-M-GL Ueye, IDS imaging, Obersulm, D; equipped with Computar MACRO 10×, Tokyo, J). In order to keep the printed sample in the camera area of observation it was constrained to a net positioned immediately above the magnetic stirrer.

3. Results and discussion

Clinical studies carried out to evaluate TMP efficacy in the treatment of severe exacerbations of asthma involved the use of IR tablet containing 25 or 50 mg of the drug [https://clinicaltrials.gov/ct2/show/NCT04049175]. Due to its very low solubility, TMP was crystallized into sub-micron sized crystals (Dv90 < 1 μm), then isolated into larger particles by spherical agglomeration technology in order to achieve better powder handling and flow properties, as highlighted in Fig. 2.

The dissolution specification for release of clinical batches, evaluated under purposely developed sink conditions test, entailed that ≥80% of the drug was liberated from the tablet in 30 min. The raw material and the dissolution specifications above described were used in the present study, which was intended to preliminarily assess an innovative manufacturing alternative that could be viable for drug product customization.

3.1. Screening of formulations

The first part of this research was aimed at investigating any impact of formulation and FDM processing conditions on the drug liberation rate.

The manufacturing of products meeting the desired dissolution specification (*i.e.* $t_{80\%} \leq 30$ min) *via* extrusion-based hot-processing techniques would be particularly challenging, because these are well-known to provide high density products characterized by slow penetration of aqueous fluids [Casati et al., 2020; Fuenmayor et al., 2019;

Table 7
Mass, TMP content and photographs of PVA-based prototypes having diverse geometries and printed with different infill percentages.

	50% infill			30% infill		
		Weight, mg (CV)	TMP strength, mg (CV)		Weight, mg (CV)	TMP strength, mg (CV)
Cylinder	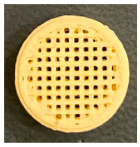	250.0 (2.39)	48.41 (2.90)		244.12 (3.18)	48.60 (3.77)
Swivel		248.07 (5.91)	47.84 (4.51)		244.36 (3.94)	45.74 (4.25)
Hexagon	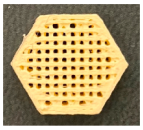	245.19 (4.03)	46.24 (4.46)	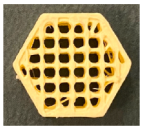	252.15 (2.87)	49.04 (2.32)
Company logo	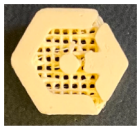	246.46 (5.01)	50.97 (4.36)	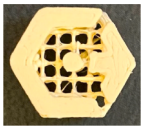	257.87 (4.28)	51.55 (4.39)
Drop		246.72 (3.72)	48.28 (3.97)	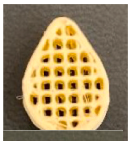	240.49 (4.30)	46.46 (3.89)
Spiral drop		249.86 (2.95)	48.08 (3.87)		256.18 (4.58)	49.54 (3.71)

Tanaka et al., 2021; Van Renterghem et al., 2018; Verstraete et al., 2016; Zema et al., 2012]. A screening program for the identification of thermoplastic carriers suitable for FDM of solid units having a dissolution performance comparable to that of reference tablets was undertaken, taking into account a variety of polymers already deemed suitable for hot-processing [Hardung et al., 2010; Melocchi et al., 2016; Nunes et al., 2022, Tanno et al., 2004]. The polymers chosen were hydrophilic in nature, either promptly soluble (*i.e.* KIR) or low-viscosity swellable/soluble ones (*e.g.* HPC), except for HPMCAS showing a pH dependent solubility profile, but being among the most efficient carriers in the preparation of solid dispersions *via* hot-processing. When multiple grades were available, polymers having the lowest molecular weight grade within the relevant family were considered (*i.e.* PVA and HPC). In most cases, it was necessary to include plasticizers into the formulation, the type and amount of which were first selected in view of literature data and then adjusted according to *i)* the behavior under extrusion of filaments with defined dimensional details/requirements and *ii)* the feeding chance of the extruded filaments into the FDM equipment during printing attempts towards the manufacturing of screening cylindrical specimens [Melocchi et al., 2016]. The versatility of formulations in terms of FDM processability was explored by *i)* setting different infill percentages (*i.e.* 100, 50 and 30%) and removing top and bottom layers to directly make available the portion involved in the infill change to fluid contact (Fig. 1), *ii)* varying the amount of TMP in the 5–40% *w*/w concentration range (*i.e.* about 5–150 mg per unit), and *iii)* adding soluble fillers. In particular, trials on PVA formulations containing up to 30% of dextrates (EMD), dextrins (TCK) and isomalt (GIQ), selected in view of preliminary literature findings, and the maximum 40% drug load were carried out [Islamipour et al., 2022]. While increasing the drug and/or the filler load, the amount of plasticizer was fine-tuned if necessary.

Main results relevant to printed screening cylindrical items are summarized in Table 3. Overall, the FDM-related steps, *i.e.* loading of the filament and relevant deposition in layers, were more challenging than the filament extrusion. In fact, although extruded filaments were obtained with all the formulations under investigation, irrespective of the TMP content, some of them needed to be discarded, resulting particularly critical for 3D printing. More into detail, the PEO-based formulations did not require the addition of any plasticizer to be extruded as they were already quite soft. However, relevant filaments showed a tendency to deform at room temperature and to stick to any type of surfaces, thus being hard to be fed into the printer. Dealing with KVA-based formulation, same sticking problems were encountered despite changing type and amount of plasticizer. However, plasticizer-free formulations could hardly be extruded due to the achievement of very high torque values (> 200 N·cm). The torque measured for HPC- and HPMCAS-based formulations was observed to progressively rise when increasing the drug load, which was associated to higher melt viscosity due to the greater presence of solid particles. During FDM this resulted in nozzle clogging so as only the formulations containing 5% of TMP turned out printable. Finally, with regard to PVA-based formulations containing 30% of soluble fillers and increasing amounts of TMP,

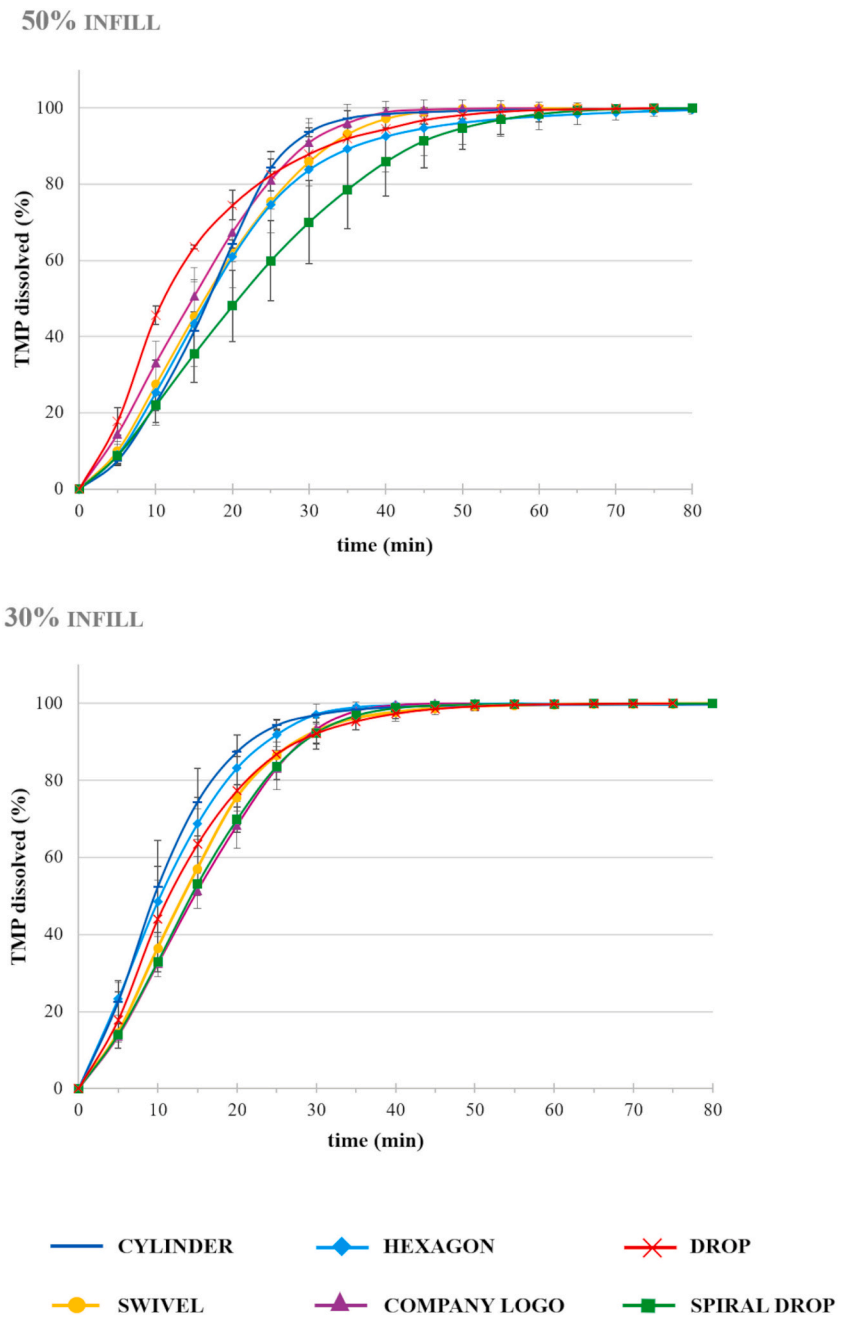

Fig. 9. dissolution profiles relevant to PVA-based samples having diverse geometries.

screening prototypes could be successfully printed following an increase in the FDM temperatures.

Overall, the aspect of the screening specimens obtained turned out satisfactory and they also pointed out a reproducible weight (CV < 10%), which was associated with good printability of the formulations. Also the actual drug content resulted close to the nominal one (CV < 5%). As far as the dissolution performance was concerned, following contact with the dissolution medium, HPMCAS- and SLP-based samples underwent a glass transition with the formation of a slowly dissolving/eroding swollen matrix. Accordingly, the TMP release rate from these systems was relatively slow (*i.e.* < 50% of drug released after 120 min for all the infill %). Considering HPC-, KIR- and PVA-based formulations, as the sample infill decreased and, for some formulations, TMP loading increased, printed screening specimens turned out able to fulfill the dissolution criterion. On the contrary, only very few samples printed with 100% infill could reach a $t_{80\%}$ < 120 min (*i.e.* test duration). Regarding the addition of soluble fillers, these showed the ability to increase the dissolution rate from the screening samples only in few cases (*i.e.* in the printed systems with 100% infill and the lowest TMP load). This was attributed to the solubility of TMP in the dissolution medium selected, forcibly increased to maintain sink conditions.

3.2. Insights on PVA-based screening samples

The screening trials were successful in highlighting formulations based on PVA as an acceptable compromise among *i)* versatility in terms of TMP content and type/amount of adjuvants, *ii)* processability by FDM, especially in terms of number of samples attained without interruptions (*e.g.* for cleaning the nozzle), *iii)* overall quality of the printed specimens and *iv)* potential towards the achievement of the dissolution target. Therefore, a further evaluation on the influence of solid state of the drug following hot-processing and impact of density/

porosity of printed samples on their dissolution performance was carried out. To this aim, in addition to 100% and 30% infill previously described, the case of 50% infill was also considered.

3.2.1. Processing conditions and solid state of TMP

TMP powder (50 mg samples) pointed out a $t_{80\%}$ value of 9.90 min (CV = 5.48). In Table 4 the dissolution results relevant to PVA-based screening specimens having 30% infill and to extruded as well as milled (< 355 μm size fraction) extruded samples, having same composition and analogous weight, are reported. When considering filaments and printed units, a slow penetration through the matrix formed by the hot-processed polymeric formulation was expected. In this respect, the $t_{80\%}$ data (*i.e.* < 20 min) relevant to printed screening specimens turned out very promising. Such a result could mainly be attributed to the increase in the surface area available for interaction with aqueous fluids, created by printing with a relatively low infill. In fact, comparing sample having the same composition, in which the active ingredient was found to maintain its original crystallinity after hot-processing and even milling (Fig. 3), the surface available for interaction with the dissolution medium seemed to represent the main cause of the differences found.

Indeed, TMP solid state following the different stages of sample manufacturing was evaluated. Accordingly, DSC analyses were performed. Neat TMP and PVA, PVA plasticized with glycerol, physical mixtures, extruded and printed samples were heated up to 325 °C. In Fig. 3a, the resulting thermograms are shown (by way of example curves relevant to the formulation containing 25% TMP are included). TMP melting, occurring approximately at 300 °C, was highlighted not only in the physical mixtures but also in the specimens prepared by HME and FDM, although occurring as a broadened endothermic peak and at lower temperatures compared to the neat drug, reasonably due to the presence of other components in the formulation. On the other hand, stability of the PVA-based formulations at the working temperatures reached during HME and FDM was investigated by means of a second DSC protocol comprising a sequence of heating and cooling, followed by a second heating step to resemble the thermal treatment the material underwent during relevant hot-processing. Notably, thermograms relevant to the first and second heating scans of the physical mixtures did not differ between each other and from those attained when first heating the corresponding extruded and printed samples. Moreover, no additional signals were detected. By way of example, data of the formulation containing 5% TMP are summarized in Fig. 3b.

XRD experiments were also performed to confirm the crystalline state of TPM in hot-processed samples. Diffractograms reported in Fig. 4, showing diffraction peaks corresponding to those of neat TPM in both extruded and printed specimens at all the percentages considered, confirmed that no major physical changes occurred on the drug during relevant hot-processing.

3.2.2. Porosity

In order to have a better insight into the dissolution performance, porosity of the printed specimens was calculated relying on pycnometric volume measurements.

Pycnometric density and porosity values of PVA-based printed screening specimens containing 5, 25 and 40% of TMP are reported in Table 5, together with the relevant mass data. Photographs of such samples are also reported in Fig. 5. The geometric volume of the screening specimens, which were printed starting from the same CAD file, turned out 363.67 mm^3 (CV = 6.85), analogous for all the samples independent of the amount of TMP conveyed in the formulation and their printing infill.

The mass of printed screening specimens having the same infill turned out decreasing for increasing nominal TMP content in the feedstock material. This finding could be an issue when targeting a specific drug load in the final prototypes. However, in view of the good printability of the formulation, the final mass of the product, and therefore the amount of drug conveyed, could be fine-tuned by changing the electronic model. The observed mass reduction could be attributed to an increase in the viscosity when dealing with formulations having an increasing content of drug particles dispersed into the polymeric carrier. The mass relevant to 50 and 30% infill specimens turned out reduced in the 42–46 and 55–62% range with respect to samples of analogous composition printed with 100% infill. This discrepancy was related to the fact that the infill changes only affected the central part and not the external shell of the printed products.

Overall, the pycnometric density resulted comparable for all the specimens, irrespective of their drug load and infill, which would indicate that open (*i.e.* accessible to the gas) voids were likely generated during printing.

The porosity of printed products, resulting from geometric and pycnometric volume measurements, was confirmed to be mainly affected by the infill set during manufacturing. Moreover, it was also highlighted an increase in the porosity correlated with the amount of TMP in the printed formulation. Indeed, the presence of the drug solid particles would create a certain stress during cooling and consolidation of the deposited layers, possibly resulting in the formation of the above-mentioned voids [Tao et al., 2021]. Such voids would contribute to the overall porosity of the items, being added up to that associated with the infill percentage set. Accordingly, a certain porosity (≤ 25%) was also measured in samples with nominal 100% infill, with a trend consistent with the TMP load. Moreover, increased porosity values were found for 50 and 30% infill samples, that turned out not markedly different between each other, probably due to the fact that only the central part and not the external shell was affected when printing with different infills.

3.2.3. Dissolution

TMP dissolution profiles from PVA-based printed samples having diverse infill and formulation are reported in Fig. 6, along with that relevant to the drug powder as such for comparison purposes. Furthermore, the dissolution rate was estimated and the resulting profiles are highlighted in Fig. 7. With respect to the reference dissolution performance of the tablet product already under clinical phase III study ($t_{80\%}$ ≥ 30 min), all the specimens printed with 50 and 30% infill turned out compliant.

As expected, TMP powder showed the highest dissolution rate, being completely dissolved within 30 min. On the other hand, drug dissolution rate from printed samples should be a function of the surface exposed to the aqueous fluids and would depend on both specimen porosity and amount of the active ingredient conveyed. Accordingly, the results obtained confirmed the slower TMP dissolution from those specimens. Focusing on the dissolution rate relevant to the first few time points, it was generally shown to increase with the TMP load, for samples having the same infill, and when the porosity increased in the case of systems based on the same formulation.

Specimens having 100% infill pointed out dissolution profiles clearly indicating an underlying control on drug release, the kinetic of which resembled that of hydrophilic prolonged release matrices. Indeed, these units were observed to slowly swell and erode upon contact with the medium, and their dissolution rate was inversely associated with the PVA content (Fig. 8). In particular, the fastest rate was observed for the 40% TMP samples, suggesting a major contribution of the erosion phenomena on the release of the drug.

Reducing the infill percentage, thus in principle increasing the openings in the central part of the unit, led to a sharp increase in the TMP release rate, progressively levelling the differences related to drug content. This result could be attributed to the different behavior of 50% and 30% infill specimens if compared to 100% ones. Indeed, during the test, they showed an early collapse and then the removal of the central portion, followed by a relatively slower erosion / solubilization of the outer shell (Fig. 8). The high percentage of voids already created when setting 50% infill (> 45%) resulted in a greater surface exposed by the central part of the item and allowed the penetration of the dissolution medium from multiple fronts, thus causing the rapid rupture of this

portion of the specimen.

In light of this peculiar behavior, the further reduction of the infill from 50 to 30% had only a limited impact on the dissolution rate. In fact, differences possibly ascribed to the infill could be highlighted in the dissolution rate profiles only at the very beginning.

As already observed to a greater extent for 100% infill specimens, increasing the TMP content seemed to enhance the erosive behavior of the formulation in view of its solubility in the dissolution medium, thus speeding up to the overall drug release. Such a consideration, more than the differences in porosity, might explain the higher initial release rate observed for 40% TPM systems, at both 50 and 30% infill.

3.3. Shape selection

The final step of the screening activity aimed at demonstrating the potential of FDM for the manufacturing of IR dosage forms containing TMP, especially devised for therapy customization. A few strategic conditions to be fulfilled for the product design were defined. In this respect, the final dosage form should:

(i) Nbe printed starting from the filament based on PVA and containing 25% TMP, as the best trade-off between process time and dosing flexibility;
(ii) exhibit an average weight of 250 mg thus conveying, in view of the formulation previously selected, nominal 50 mg of TMP. Indeed, this would represent the highest nominal drug content among the proposed therapeutic dosages;
(iii) fulfill the dissolution specification, *i.e.* $t_{80\%} \leq 30$ min;
(iv) entail a compliant shape/geometry, *e.g.* simple to be handled and easy to be identified from the patient perspective, and possibly contribute to strengthen the brand identity.

Having these criteria in mind, various shapes and only 50 and 30% infill were considered, as summarized in Table 6. To favor swallowing and compliance, some dimensional constraints were implemented. In this respect, the main diameter/width of the final prototypes was established to be smaller than 14 mm. Therefore, height of the printed units with 30% infill needed to be increased to attain the same TMP load. A cylindrical shape was first chosen, being particularly simple to print and similar to the screening prototypes previously built. Moreover, by adapting the diameter/height ratio it could also be acceptable from the patient point of view. A drop-like geometry was also taken into account in view of the relatively higher swallowing compliance it is expected to provide [Fastø et al., 2019]. In both these cases, two additional alternatives were designed, willing to increase as much as possible the surface area available for interaction with aqueous fluids (*i.e.* swivel and spiral drop). Finally, to enhance product identification with the industry brand, a complex hexagon-like shape recalling the company logo was also conceived.

As the formulation was previously studied, HME and FDM parameters were not changed with respect to those already discussed. Weight data turned out particularly reproducible and even the target TMP content was achieved, thus confirming the good FDM processability of the formulation in use also when dealing with more complex shapes (Table 7). Cylindrical samples, being based on the less complex virtual model, showed the best resolution and higher reproducibility in terms of weight. Increasing the height for samples printed with 30% infill resulted in an increased number of shells overlapping in the z axis in the final units, thus leading to a continuous external surface. This could impact on the unit dissolution performance. All the prototypes designed were basically able to meet the dissolution specification, thus leaving the possibility to choose, during product development stages and eventually based on preliminarily patient preference studies, the most compliant shape (Fig. 9). On the latter it would be also possible to enhance the effective surface available for interaction with aqueous fluids.

4. Conclusions

The development of an oral 3D printed IR dosage form *via* FDM containing TMP and with a potential towards patient-centric therapy was successful. The prototypes were fabricated starting from a selected PVA-based formulation and were characterized by diverse TMP dosages and patient-compliant shapes. Moreover, they met the dissolution specification set, showing a performance comparable to that of the reference tablet product already approved for clinical phase III studies. Once again, the FDM was demonstrated an economic tool for speeding up pharmaceutical product innovation and customization in terms of drug dose, formulation and product design. Moreover, in this work the use of pycnometric analyses was proposed to deepen the role of the infill on the dissolution performance of printed specimens, which could be implemented in the R&D stages of personalized IR dosage forms manufactured by FDM.

Declaration of Competing Interest

None.

Data availability

Data will be made available on request.

Acknowledgment

We would like to thank Franco Sartor and Guido Bellazzi for their support in solid state analyses.

References

Aho, J., Bøtker, J.P., Genina, N., Edinger, M., Arnfast, L., Rantanen, J., 2019. Roadmap to 3D-printed oral pharmaceutical dosage forms: feedstock filament properties and characterization for fused deposition modeling. J. Pharm. Sci. 108, 26–35.
Arafat, B., Wojsz, M., Isreb, A., Forbes, R.T., Isreb, M., Ahmed, W., Arafat, T., Alhnan, M. A., 2018. Tablet fragmentation without a disintegrant: a novel design approach for accelerating disintegration and drug release from 3D printed cellulosic tablets. Eur. J. Pharm. Sci. 118, 191–199.
Cailleaux, S., Sanchez-Ballester, N.M., Gueche, Y.A., Bataille, B., Soulairol, I., 2021. Fused Deposition Modeling (FDM), the new asset for the production of tailored medicines. J. Control. Release 330, 821–841.
Casati, F., Melocchi, A., Moutaharrik, S., Uboldi, M., Foppoli, A., Maroni, A., Zema, L., Neut, C., Siepmann, F., Siepmann, J., Gazzaniga, A., 2020. Injection molded capsules for colon delivery combining time-controlled and enzyme-triggered approaches. Int. J. Mol. Sci. 21, 1917.
Crișan, A.G., Iurian, S., Porfire, A., Rus, L.M., Bogdan, C., Casian, T., Lucacel, R.C., Turza, A., Porav, S., Tomuță, I., 2022. QbD guided development of immediate release FDM-3D printed tablets with customizable API doses. Int. J. Pharm. 613, 121411.
Curti, C., Kirby, D.J., Russel, C.A., 2020. Current formulation approaches in design and development of solid oral dosage forms through three-dimensional printing. Prog. Addit. Manuf. 5, 111–123.
Dos Santos, J., Deon, M., Da Silva, G.S., Beck, R.C.R., 2021. Multiple variable effects in the customisation of fused deposition modelling 3D-printed medicines: a design of experiments (DoE) approach. Int. J. Pharm. 597, 120331.
Dumpa, N., Butreddy, A., Wang, H., Komanduri, N., Bandari, S., Repka, M.A., 2021. 3D printing in personalized drug delivery: an overview of hot-melt extrusion-based fused deposition modeling. Int. J. Pharm. 600, 120501.
Duranović, M., Madžarević, M., Ivković, B., Ibrić, S., Cvijić, S., 2021. The evaluation of the effect of different superdisintegrants on the drug release from FDM 3D printed tablets through different applied strategies: in vitro-in silico assessment. Int. J. Pharm. 610, 121194.
Edinger, M., Jacobsen, J., Bar-Shalom, D., Rantanen, J., Genina, N., 2018. Analytical aspects of printed oral dosage forms. Int. J. Pharm. 553, 97–108.
Elbadawi, M., Muñiz, Castro B., Gavins, F.K.H., Ong, J.J., Gaisford, S., Pérez, G., Basit, A. W., Cabalar, P., Goyanes, A., 2020. M3DISEEN: a novel machine learning approach for predicting the 3D printability of medicines. Int. J. Pharm. 590, 119837.
Elbadawi, M., McCoubrey, L.E., Gavins, F.K.H., Ong, J.J., Goyanes, A., Gaisford, S., Basit, A.W., 2021a. Disrupting 3D printing of medicines with machine learning, Trends in Pharm. Sci. 42, 745–757.
Elbadawi, M., McCoubrey, L.E., Gavins, F.K.H., Ong, J.J., Goyanes, A., Gaisford, S., Basit, A.W., 2021b. Harnessing artificial intelligence for the next generation of 3D printed medicines. Adv. Drug Deliv. Rev. 175, 113805.

Fanous, M., Gold, S., Hirsch, S., Ogorka, J., Imanidis, G., 2020. Development of immediate release (IR) 3D-printed oral dosage forms with focus on industrial relevance. Eur. J. Pharm. Sci. 155, 105558.
Fanous, M., Bitar, M., Gold, S., Sobczuk, A., Hirsch, S., Ogorka, J., Imanidis, G., 2021. Development of immediate release 3D-printed dosage forms for a poorly water-soluble drug by fused deposition modeling: Study of morphology, solid state and dissolution. Int. J. Pharm. 599, 120417.
Fastø, M.M., Genina, N., Kaae, S., Kälvemark, Sporrong S., 2019. Perceptions, preferences and acceptability of patient designed 3D printed medicine by polypharmacy patients: a pilot study. Int. J. Clin. Pharm. 41, 1290–1298.
Fuenmayor, E., Forde, M., Healy, A.V., Devine, D.M., Lyons, J.G., McConvill, C., Major, I., 2018. Material considerations for fused-filament fabrication of solid dosage forms. Pharmaceutics 10, 44.
Fuenmayor, E., Forde, M., Healy, A.V., Devine, D.M., Lyons, J.G., McConville, C., Major, I., 2019. Comparison of fused-filament fabrication to direct compression and injection molding in the manufacture of oral tablets. Int. J. Pharm. 558, 328–340.
Goyanes, A., Buanz, A.B.M., Hatton, G.B., Gaisford, S., Basit, A.W., 2015a. 3D printing of modified-release aminosalicylate (4-ASA and 5-ASA) tablets. Eur. J. Pharm. Biopharm. 89, 157–162.
Goyanes, A., Wang, J., Buanz, A., Martínez-Pacheco, R., Telford, R., Gaisford, S., Basit, A. W., 2015b. 3D printing of medicines: engineering novel oral devices with unique design and drug release characteristics. Mol. Pharm. 12, 4077–4084.
Goyanes, A., Robles, Martinez P., Buanz, A., Basit, A.W., Gaisford, S., 2015c. Effect of geometry on drug release from 3D printed tablets. Int. J. Pharm. 494, 657–663.
Gültekin, H.E., Tort, S., Acartürk, F., 2019. An effective technology for the development of immediate release solid dosage forms containing low-dose drug: fused deposition modeling 3D printing. Pharm. Res. 36, 128.
Gupta, D.K., Ali, M.H., Ali, A., Jain, P., Anwer, M.K., Iqbal, Z., Mirza, M.A., 2022. 3D printing technology in healthcare: applications, regulatory understanding, IP repository and clinical trial status. J. Drug Target. 30, 131–150.
Hardung, H., Djuric, D., Ali, S., 2010. Combining HME & solubilization: Soluplus® - the solid solution, Drug Deliv. Tech. 10, 20–27.
Henry, S., De Wever, L., Vanhoorne, V., De Beer, T., Vervaet, C., 2021. Influence of print settings on the critical quality attributes of extrusion-based 3d-printed caplets: A quality-by-design approach. Pharmaceutics 13, 2068. https://www.chiesi.com/img/annual_report/documenti/mZQpMHoqnWAnR_2016_ENG_SD.pdf. last access on July 29, 2022 https://clinicaltrials.gov/ct2/show/NCT04049175, last access on July 29, 2022.
Ilyés, K., Kovács, N.K., Balogh, A., Borbás, E., Farkas, B., Casian, T., Marosi, G., Tomuță, I., Nagy, Z.K., 2019. The applicability of pharmaceutical polymeric blends for the fused deposition modelling (FDM) 3D technique: Material considerations–printability–process modulation, with consecutive effects on in vitro release, stability and degradation. Eur. J. Pharm. Sci. 129, 110–123.
Islamipour, Z., Zare, E.N., Salimi, F., Ghomi, M., Makvandi, P., 2022. Biodegradable antibacterial and antioxidant nanocomposite films based on dextrin for bioactive food packaging. J. Nanostruct. Chem. https://doi.org/10.1007/s40097-022-00491-4.
Isreb, A., Baj, K., Wojsz, M., Isreb, M., Peak, M., Alhnan, M.A., 2019. 3D printed oral theophylline doses with innovative 'radiator-like' design: Impact of polyethylene oxide (PEO) molecular weight. Int. J. Pharm. 564, 98–105.
Joo, Y., Shin, I., Ham, G., Abuzar, S.M., Hyun, S.-M., Hwang, S.-J., 2020. The advent of a novel manufacturing technology in pharmaceutics: superiority of fused deposition modeling 3D printer. J. Pharm. Inv. 50, 131–145.
Krueger, L., Miles, J.A., Popat, A., 2022. 3D printing hybrid materials using fused deposition modelling for solid oral dosage forms. J. Control. Release 351, 444–455.
Li, P., Jia, H., Zhang, S., Yang, Y., Sun, H., Wang, H., Pan, W., Yin, F., Yang, X., 2020. Thermal Extrusion 3D printing for the fabrication of puerarin immediate-release tablets. AAPS PharmSciTech 21, 20.
Linares, V., Galdón, E., Casas, M., Caraballo, I., 2021. Critical points for predicting 3D printable filaments behavior. J. Drug Deliv. Sci. Technol. 66, 102933.
Lommatzsch, M., 2020. Immune modulation in asthma: current concepts and future strategies. Respiration 99, 566–576.
Markl, D., Zeitler, A., Rades, T., Rantanen, J., Bøtker, J., 2018. Toward quality assessment of 3D printed oral dosage forms, J. 3D Print. Med. 2, 27–33.
Maroni, A., Melocchi, A., Zema, L., Foppoli, A., Gazzaniga, A., 2020. Retentive drug delivery systems based on shape memory materials. J. Appl. Polym. Sci. 137, 48798.
Melocchi, A., Parietti, F., Maroni, A., Foppoli, A., Gazzaniga, A., Zema, L., 2016. Hot-melt extruded filaments based on pharmaceutical grade polymers for 3D printing by fused deposition modeling. Int. J. Pharm. 509, 255–263.
Melocchi, A., Inverardi, N., Uboldi, M., Baldi, F., Maroni, A., Pandini, S., Briatico-Vangosa, F., Zema, L., Gazzaniga, A., 2019a. Retentive device for intravesical drug delivery based on water-induced shape memory response of poly(vinil alcohol): design concept and 4D printing feasibility. Int. J. Pharm. 559, 299–311.
Melocchi, A., Uboldi, M., Inverardi, N., Briatico-Vangosa, F., Baldi, F., Pandini, S., Scalet, G., Auricchio, F., Cerea, M., Foppoli, A., Maroni, A., Zema, L., Gazzaniga, A., 2019b. Expandable drug delivery system for gastric retention based on shape memory polymers: development via 4D printing and extrusion. Int. J. Pharm. 571, 118700.
Melocchi, A., Uboldi, M., Cerea, M., Foppoli, A., Maroni, A., Moutaharrik, S., Palugan, L., Zema, L., Gazzaniga, A., 2020a. A graphical review on the escalation of fused deposition modeling (FDM) 3D printing in the pharmaceutical field, J. Pharm. Sci. 109, 2943–2957.
Melocchi, A., Uboldi, M., Parietti, F., Cerea, M., Foppoli, A., Palugan, L., Gazzaniga, A., Maroni, A., Zema, L., 2020b. Lego-inspired capsular devices for the development of personalized dietary supplements: proof of concept with multimodal release of caffeine. J. Pharm. Sci. 109, 1990–1999.
Melocchi, A., Briatico-Vangosa, F., Uboldi, M., Parietti, F., Turchi, M., von Zeppelin, D., Maroni, A., Zema, L., Gazzaniga, A., Zidan, A., 2021a. Quality considerations on the pharmaceutical applications of fused deposition modeling 3D printing. Int. J. Pharm. 592, 119901.
Melocchi, A., Uboldi, M., Cerea, M., Foppoli, A., Maroni, A., Moutaharrik, S., Palugan, L., Zema, L., Gazzaniga, A., 2021b. Shape memory materials and 4D printing in pharmaceutics. Adv. Drug Deliv. Rev. 173, 216–237.
Melocchi, A., Uboldi, M., Briatico-Vangosa, F., Moutaharrik, S., Cerea, M., Foppoli, A., Maroni, A., Palugan, L., Zema, L., Gazzaniga, A., 2021c. The Chronotopic™ system for pulsatile and colonic delivery of active molecules in the era of precision medicine: Feasibility by 3D printing via fused deposition modeling (FDM). Pharmaceutics 13, 759.
Muñiz, Castro B., Elbadawi, M., Ong, J.J., Pollard, T., Song, Z., Gaisford, S., Pérez, G., Basit, A.W., Cabalar, P., Goyanes, A., 2021. Machine learning predicts 3D printing performance of over 900 drug delivery systems. J. Control. Release 337, 530–545.
Nunes, P.D., Pinto, J.F., Henriques, J., Paiva, A.M., 2022. Insights into the release mechanisms of ITZ:HPMCAS amorphous solid dispersions: the role of drug-rich colloids. Mol. Pharm. 19, 1.
Okwuosa, T.C., Sadia, M., Isreb, A., Habashy, R., Peak, M., Alhnan, M.A., 2021. Can filaments be stored as a shelf-item for on-demand manufacturing of oral 3D printed tablets? An initial stability assessment. Int. J. Pharm. 600, 120442.
Palugan, L., Cerea, M., Cirilli, M., Moutaharrik, S., Maroni, A., Zema, L., Melocchi, A., Uboldi, M., Filippin, I., Foppoli, A., Gazzaniga, A., 2021. Intravesical drug delivery approaches for improved therapy of urinary bladder diseases. Int. J. Pharm. X 3, 100100.
Parulski, C., Jennotte, O., Lechanteur, A., Evrard, B., 2021. Challenges of fused deposition modeling 3D printing in pharmaceutical applications: where are we now? Adv. Drug Deliv. Rev. 175, 113810.
Pires, F.Q., Alves-Silva, I., Pinho, L.A.G., Chaker, J.A., Sa-Barreto, L.L., Gelfuso, G.M., Gratieri, T., Cunha-Filho, M., 2020. Predictive models of FDM 3D printing using experimental design based on pharmaceutical requirements for tablet production. Int. J. Pharm. 588, 119728.
Quodbach, J., Bogdahn, M., Breitkreutz, J., Chamberlain, R., Eggenreich, K., Elia, A.G., Gottschalk, N., Gunkel-Grabole, G., Hoffmann, L., Kapote, D., Kipping, T., Klinken, S., Loose, F., Marquetant, T., Windolf, H., Geißler, S., Spitz, T., 2022. Quality of FDM 3D printed medicines for pediatrics: considerations for formulation development, filament extrusion, printing process and printer design. Ther. Innov. Regul. Sci. 56, 910–928.
Sadia, M., Sośnicka, A., Arafat, B., Isreb, A., Ahmed, W., Kelarakis, A., Alhnan, M.A., 2016. Adaptation of pharmaceutical excipients to FDM 3D printing for the fabrication of patient-tailored immediate release tablets. Int. J. Pharm. 513, 659–668.
Sadia, M., Arafat, B., Ahmed, W., Forbes, R.T., Alhnan, M.A., 2018. Channelled tablets: an innovative approach to accelerating drug release from 3D printed tablets. J. Control. Release 269, 355–363.
Seoane-Viaño, I., Trenfield, S.J., Basit, A.W., Goyanes, A., 2021. Translating 3D printed pharmaceuticals: from hype to real-world clinical applications. Adv. Drug Deliv. Rev. 174, 553–575.
Shaqour, B., Samaro, A., Verleije, B., Beyers, K., Vervae, C., Cos, P., 2020. Production of drug delivery systems using fused filament fabrication: a systematic review. Pharmaceutics 12, 517.
Shi, K., Slavage, J.P., Maniruzzaman, M., Nokhodchi, A., 2021. Role of release modifiers to modulate drug release from fused deposition modelling (FDM) 3D printed tablets. Int. J. Pharm. 597, 120315.
Shrimanker, R., Borg, K., Connolly, C., Thulborn, S., Cane, J., Xue, L., Hynes, G., Hinks, T., Kots, M., Girardello, L., Petruzzelli, S., Steiner, J., Vinall, S., Hunter, M., Pettipher, R., Pavord, I.D., 2019. Effect of timapiprant, a DP2 antagonist, on airway inflammation in severe eosinophilic asthma. Eur. Respir. J. 54, 63.
Singh, D., Cadden, P., Hunter, M., Pearce, Collins L., Perkins, M., Pettipher, R., Townsend, E., Vinall, S., O'Connor, B., 2013. Inhibition of the asthmatic allergen challenge response by the CRTH2 antagonist OC000459. Eur. Respir. J. 41, 46–52.
Smith, D., Kapoor, Y., Hermans, A., Nofsinger, R., Kesisoglou, F., Gustafson, T.P., Procopio, A., 2018a. 3D printed capsules for quantitative regional absorption studies in the GI tract. Int. J. Pharm. 550 (2), 418–428.
Smith, D.M., Kapoor, Y., Klinzing, G.R., Procopio, A.T., 2018b. Pharmaceutical 3D printing: design and qualification of a single step print and fill capsule. Int. J. Pharm. 544, 21–30.
Solanki, N.G., Tahsin, M., Shah, A.V., Serajuddin, A.T.M., 2018. Formulation of 3D printed tablet for rapid drug release by fused deposition modeling: screening polymers for drug release, drug-polymer miscibility and printability. J. Pharm. Sci. 107, 390–401.
Tagami, T., Fukushige, K., Ogawa, E., Hayashi, N., Ozeki, T., 2017. 3D Printing factors important for the fabrication of polyvinylalcohol filament-based tablets. Biol. Pharm. Bull. 40, 357–364.
Tan, D.K., Maniruzzaman, M., Nokhodchi, A., 2018. Advanced pharmaceutical applications of hot-melt extrusion coupled with fused deposition modelling (FDM) 3D printing for personalised drug delivery. Pharmaceutics 10, 203.
Tanaka, R., Ishihara, S., Sasaki, T., Hattori, Y., Otsuka, M., 2021. Injection-molded coamorphous tablets: analysis of intermolecular interaction and crystallization propensity. J. Pharm. Sci. 110, 3289–3297.
Tanno, F., Nishiyama, Y., Kokubo, H., Obara, S., 2004. Evaluation of hypromellose acetate succinate (HPMCAS) as a carrier in solid dispersions. Drug Dev. Ind. Pharm. 30, 9–17.
Tao, Y., Kong, F., Li, Z., Zhang, J., Zhao, X., Yin, Q., Xing, D., Li, P., 2021. A review on voids of 3D printed parts by fused filament fabrication. J. Mater. Res. Technol. 15, 4860–487.

Than, Y.M., Titapiwatanakun, V., 2021. Tailoring immediate release FDM 3D printed tablets using a quality by design (QbD) approach. Int. J. Pharm. 599, 120402.
Trenfield, S.J., Goyanes, A., Telford, R., Wilsdon, D., Rowland, M., Gaisford, S., Basit, A. W., 2018. 3D printed drug products: Non-destructive dose verification using a rapid point-and-shoot approach. Int. J. Pharm. 549, 1–2.
Trenfield, S.J., Tan, H.X., Goyanes, A., Wilsdon, D., Rowland, M., Gaisford, S., Basit, A. W., 2020. Non-destructive dose verification of two drugs within 3D printed polyprintlets. Int. J. Pharm. 577, 119066.
Uboldi, M., Melocchi, A., Moutaharrik, S., Cerea, M., Gazzaniga, A., Zema, L., 2021. Dataset on a small-scale film-coating process developed for self-expanding 4D printed drug delivery devices. Coatings 11, 1252.
Uboldi, M., Melocchi, A., Moutaharrik, S., Palugan, L., Cerea, M., Foppoli, A., Maroni, A., Gazzaniga, A., Zema, L., 2022. Administration strategies and smart devices for drug release in specific sites of the upper GI tract. J. Control. Release 348, 537–552.
Van Renterghem, J., Dhondt, H., Verstraete, G., De Bruyne, M., Vervaet, C., De Beer, T., 2018. The impact of the injection mold temperature upon polymer crystallization and resulting drug release from immediate and sustained release tablets, Int. Aust. J. Pharm. 541, 108–116.
Vaz, V.M., Kumar, L., 2021. 3D printing as a promising tool in personalized medicine. AAPS PharmSciTech 22, 49.
Verstraete, G., Mertens, P., Grymonpré, W., Van Bockstal, P.J., De Beer, T., Boone, M.N., Van Hoorebeke, L., Remon, J.P., Vervaet, C., 2016. A comparative study between melt granulation/compression and hot melt extrusion/injection molding for the manufacturing of oral sustained release thermoplastic polyurethane matrices. Int. J. Pharm. 513, 602–611.
Wang, J., Zhang, Y., Aghda, N.H., Pillai, A.R., Thakkar, R., Nokhodchi, A., Maniruzzaman, M., 2021. Emerging 3D printing technologies for drug delivery devices: current status and future perspective. Adv. Drug Deliv. Rev. 174, 294–316.
Yang, Y., Wang, H., Li, H., Ou, Z., Yang, G., 2018. 3D printed tablets with internal scaffold structure using ethyl cellulose to achieve sustained ibuprofen release. Eur. J. Pharm. Sci. 115, 11–18.
Zema, L., Loreti, G., Melocchi, A., Maroni, A., Gazzaniga, A., 2012. Injection Molding and its application to drug delivery. J. Control. Release 159, 324–331.